THE JOURNAL OF PHYSICAL CHEMISTRY A

Article

pubs.acs.org/JPCA

State-to-State Differential Cross Sections for Inelastic Collisions of NO Radicals with *para*-H_2 and *ortho*-D_2

Zhi Gao, Sjoerd N. Vogels, Matthieu Besemer, Tijs Karman, Gerrit C. Groenenboom, Ad van der Avoird, and Sebastiaan Y. T. van de Meerakker*

Radboud University, Institute for Molecules and Materials, Heyendaalseweg 135, 6525 AJ, Nijmegen, The Netherlands

ABSTRACT: We present state-to-state differential cross sections for collisions of NO molecules ($X^2\Pi_{1/2}$, $j = 1/2$f) with *para*-H_2 and *ortho*-D_2 molecules, at a collision energy of 510 and 450 cm^{-1}, respectively. The angular scattering distributions for various final states of the NO radical are measured with high resolution using a crossed molecular beam apparatus that employs the combination of Stark deceleration and velocity map imaging. Rotational rainbows as well as diffraction oscillations are fully resolved in the scattering images. The observed angular scattering distributions are in excellent agreement with the cross sections obtained from quantum close-coupling scattering calculations based on recently computed NO−H_2 potential energy surfaces, except for excitation of NO into the $j = 7/2$f channel. For this particular inelastic channel, a significant discrepancy with theory is observed, despite various additional measurements and calculations, at present, not understood.

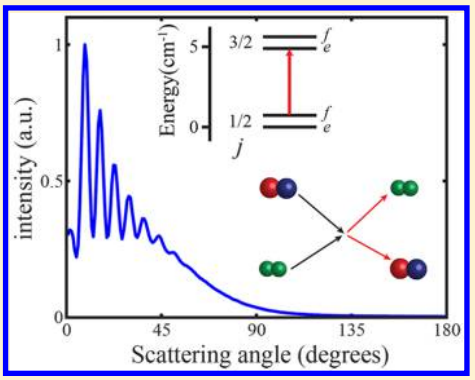

1. INTRODUCTION

Crossed molecular beam scattering provides one of the most accurate and widely used approaches to probe the interactions between gas-phase particles.[1] These interactions can be theoretically described by potential energy surfaces (PESs) that can be *ab initio* calculated using quantum mechanical methods. Experimentally determined integral and differential cross sections (ICSs and DCSs) are sensitive probes of the PES. Comparison between experimental cross sections and cross sections derived from scattering calculations based on the PES has been a powerful strategy in the last decades to unravel the nature of molecular interactions. The ability to construct PESs with ever higher accuracy allows for the accurate prediction of cross sections and rate coefficients for a wide range of molecular processes and has large dividends in research fields ranging from atmospheric chemistry and combustion to astrochemistry.

One of the benchmark systems for studying molecular interactions is rotational energy transfer in collisions between NO radicals and rare gas atoms. Due to the open-shell nature of the NO radical, the interaction between NO and its collision partner is governed by two PESs, which are non-adiabatically coupled. This allows for the study of collision dynamics beyond the Born−Oppenheimer approximation. Rotationally inelastic collisions between NO and rare gas atoms have been studied extensively, resulting in a wealth of experimental data.[2−12] Near exact quantum scattering calculations on accurate PESs are possible, yielding scattering cross sections that are in excellent agreement with the most accurate experimental results.[2,6] Collisions of NO radicals with other molecules, however, are much less well understood. Experimentally, it is difficult to control the molecular scattering partner, and only limited data is available on bimolecular systems.[13] Theoretically, the added complexity of the nonspherical shape and internal degrees of freedom of the scattering partner renders the *ab initio* calculations and fitting of the PESs much more difficult.

As a stepping stone toward the understanding of complex bimolecular systems, collisions between NO radicals and H_2 molecules have been the subject of a number of studies. H_2 ($X\,^1\Sigma_g^+$) in its $j = 0$ rotational ground state is often regarded as the most simple molecule, and its electronic structure resembles the structure of an atom. In addition, the interaction between H_2 and other molecules plays an important role in astrophysics since H_2 is the most abundant molecule in interstellar space. Westley et al. studied differential cross sections for inelastic collisions of NO with He and D_2 for both spin−orbit conserving and spin−orbit changing transitions and found small differences in the rainbow positions between NO + He and NO + D_2.[14] By using a hexapole state selector, Gijsbertsen et al. found significant differences in rainbow positions between parity conserving and parity changing transitions.[15] Luxford et al. reported the state-to-state DCSs and angular resolved rotational angular momentum polarization moments for collisions of electronically excited NO($A^2\Sigma$) with D_2.[16] Recently, de Jongh et al. studied the DCS of NO + He and NO + *ortho*-D_2 with very high resolution as a function of the collision energy using a Stark decelerator, resolving diffraction oscillations in the angular distributions. Due to the larger size of D_2, the differences in angular spacing between individual diffraction peaks were observed.[17] Theoretically, two NO−H_2 PESs have been reported in the literature recently.[18,19]

Received: July 11, 2017
Revised: September 14, 2017
Published: September 14, 2017

DOI: 10.1021/acs.jpca.7b06808
J. Phys. Chem. A 2017, 121, 7446−7454

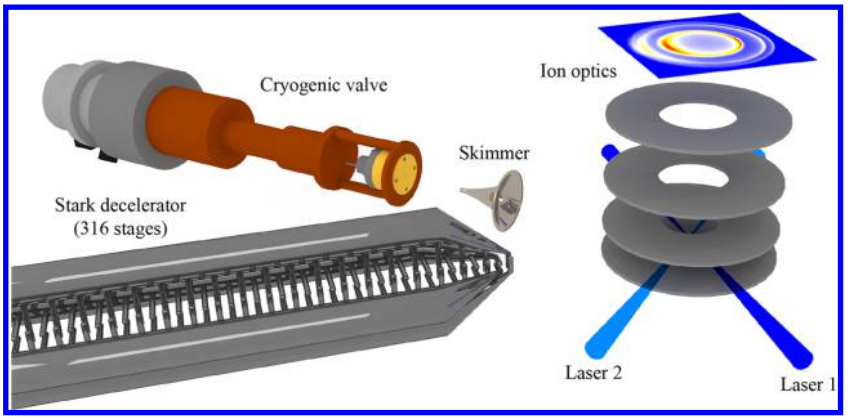

Figure 1. Schematic representation of the experimental setup. A beam of NO radicals is passed through a Stark decelerator and scattered with a pulsed beam of *para*-H_2 or *ortho*-D_2. The inelastically scattered NO radicals are state-selectively ionized using two pulsed lasers and detected using velocity map imaging. Only the last section of the Stark decelerator is shown.

In this article, we report on high-resolution measurements of inelastic collisions of NO radicals with *para*-H_2 and *ortho*-D_2 molecules at a collision energy of 510 and 450 cm^{-1}, respectively. The measurements are performed in a unique crossed beam apparatus that employs the combination of Stark deceleration and velocity map imaging.[20] DCSs are probed for a variety of inelastic scattering channels. In the scattering images, fine structures in the angular distributions such as diffraction oscillations are fully resolved. The measured angular distributions are compared to the distributions predicted by quantum close coupling scattering calculations based on the recently developed *ab initio* PESs for NO−H_2.[17] Excellent agreement between experiment and theory is obtained, except for the scattering channel where NO is excited into the (7/2f) state. This behavior is found for both NO−H_2 and NO−D_2 collisions. Despite numerous additional experimental and theoretical studies, this remarkable discrepancy remains and is, at present, unaccounted for.

2. METHODS

2.1. Experimental Setup. The crossed molecular beam scattering apparatus that is used in this work contains a Stark decelerator and velocity map imaging detector and is schematically shown in Figure 1. The operation and characterization of the Stark decelerator has been described in detail before.[20−23] A beam of NO radicals is formed by expanding a mixture of 5% NO seeded in Kr at typical 1 bar pressure from a Nijmegen Pulsed Valve.[24] After passing through the decelerator, a package of NO ($X\ ^2\Pi_{1/2}$, j = 1/2f) radicals with a mean velocity of 390 ms^{-1}, a velocity spread of 2.1 ms^{-1} (1σ), and an angular spread of 0.1° (1σ) is scattered with beams of *para*-H_2 or *ortho*-D_2 at an intersection angle of 45°. The population in the j = 0 rotational ground state for H_2 and D_2 is optimized by converting normal H_2 and D_2 into pure *para*-H_2 and *ortho*-D_2 using a *para*−*ortho* converter.[17] The H_2 and D_2 beams are produced using a room-temperature Even−Lavie valve at a pressure of 20 and 10 bar, respectively. The rotational state purity of the H_2 and D_2 beams is probed using REMPI, as described before.[17]

The NO radicals are state-selectively detected using a (1 + 1′) Resonance Enhanced MultiPhoton Ionization (REMPI) scheme. The first laser with a wavelength of 226 nm and a bandwidth of approximately 0.08 cm^{-1} can be tuned to selected rotational branches of the $A^2\Sigma^+ \leftarrow X^2\Pi$ transition to probe the scattered NO radicals in a specific final rotational (j) and Λ-doublet (e or f) state. Typical pulse energies of only about 5 μJ are used for this laser to avoid ionization by a direct (1 + 1) REMPI process. The second laser with a wavelength around 328 nm can be tuned to subsequently ionize the NO radicals at their energetic threshold to eliminate blurring effects due to electron recoil energy. A time delay of 13 ns between both lasers is kept fixed for all measurements. The second laser has a typical pulse energy of about 8 mJ and is focused into the ionization region with a spherical lens with 500 mm focal length. It is verified that all ionization signal disappears when blocking either of the two laser beams.[20]

Velocity map imaging (VMI) optics are used to collect the NO ions after the ionization. The ion optics used in the experiment consist of a repeller and three extractor plates as used by Suits and co-workers.[25] We use a grounded time-of-flight (TOF) tube of 1100 mm length in order to increase the size of the scattering images. The voltage applied on repeller and extractor plates are 3000, 2755, 2519, and 2100 V, respectively. Time-slicing was not used in the experiments; the three-dimensional Newton spheres are crushed onto the detector plane. The impinging ions are detected by a standard MCP detector in combination with a phospor screen. Scattering images are recorded using a PCO Pixelfly 270XS camera (1391 × 1023 pixels). Both event counting and centroiding is used in the data acquisition process. We carefully calibrate our velocity map imaging detector using velocity controlled beams of NO as described before,[20] and we find a calibration factor of 2.1 ms^{-1} $pixel^{-1}$. From this calibration, the mean speed for *para*-H_2 and *ortho*-D_2 is determined to be 2812 and 2000 ms^{-1}, respectively, resulting in a collision energy of 510 and 450 cm^{-1}, respectively.

2.2. Quantum Scattering Calculation. Coupled-channel or close-coupling calculations were performed to obtain the DCS for NO-*ortho*-D_2 and NO-*para*-H_2 collisions. Our scattering program for bimolecular collisions can also handle open-shell systems and was developed in Nijmegen. It uses a body-fixed channel basis, which simplifies the calculation of the matrix elements of the potential, applies a renormalized Numerov propagator in the radial coordinate R, and transforms to the usual space-fixed basis to apply S-matrix boundary conditions at large R. The Hamiltonian is the same as that described by Groenenboom et al.[26] for OH-HCl, but the molecular parameters of NO and H_2 or D_2 are different, of course. Also, the channel basis and the matrix elements are the same as in the bound state calculations of ref 26.

Two sets of PESs are currently available for NO−H_2 and are described by de Jongh et al.[17] and Kłos et al.[19] These PESs employ subtle differences in their approximations and result in

DOI: 10.1021/acs.jpca.7b06808
J. Phys. Chem. A 2017, 121, 7446−7454

minor differences at low collision energies in the calculations of the integral and differential cross sections. At the relatively high collision energies employed in this work, the resulting differences in DCSs and ICSs from the two sets of PESs are negligible. Although the vibrationally averaged bond length of D_2 differs from that of H_2, we used the same interaction potential for NO−D_2 as for NO−H_2. Hence, these two systems only differ in the reduced mass and the rotational constants. For the NO−H_2 calculations, all the partial waves that contribute up to a total angular momentum $\mathcal{J} = 40.5$ and rotational levels up to $j_{NO} = 10.5$ and $j_{H_2} = 3$ were included in the channel basis. For the NO−D_2 calculations, we included partial waves contributing to $\mathcal{J} = 60.5$ and rotational levels up to $j_{NO} = 15.5$ and $j_{D_2} = 3$. The total number of channel functions employed in these calculations amounts to more than 2500. For both the NO−H_2 and NO−D_2 scattering calculations the wave function was propagated on a radial grid ranging from $R = 4.5$ to 40 a_0 with a grid spacing of 0.1 a_0. The calculated DCSs are used as input for simulations that account for the experimental conditions.

3. RESULTS AND DISCUSSION

3.1. Procedures and Simulations. All measurements presented in this article are conducted, analyzed, and compared to theoretical calculations in the same way. To illustrate the procedures, we present in Figure 2 the results for the scattering process NO (1/2f) + *para*-H_2 → NO (3/2e) + *para*-H_2 as an example. Part of the rotational energy level diagram of NO is shown in Figure 2d, where the red arrow indicates the collision-induced rotational excitation discussed here. Only the spin−orbit conserving transitions were probed in the work presented in this article. The results for all final states and NO + D_2 collisions are presented in sections 3.2 and 3.3, respectively.

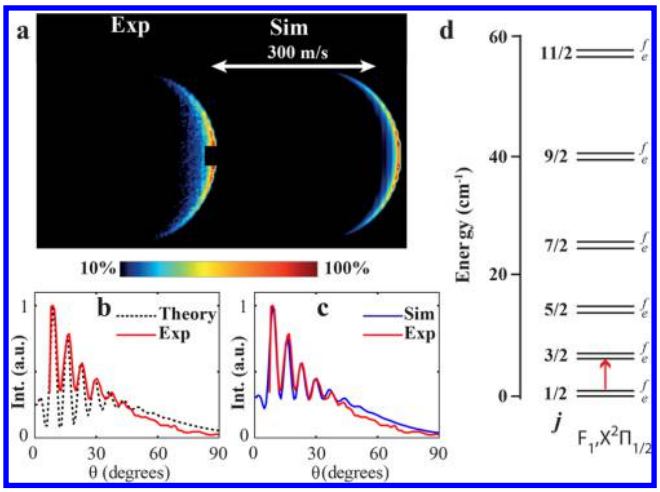

Figure 2. Results for the scattering process NO (1/2f) + *para*-H_2 → NO (3/2e) + *para*-H_2. (a) Raw experimental (left) and simulated (right) scattering image. (b) Comparison of the experimental angular scattering distribution with the DCS predicted by theory. (c) Comparison of the angular scattering distributions from the experimental and simulated images. (d) Rotational energy level diagram of NO indicating the collision-induced inelastic transition, with Λ-doubling splitting exaggerated for clarity.

The raw experimental scattering image is shown in Figure 2a. Throughout this article, images are presented such that the relative velocity vector is directed horizontally, with forward scattered angles positioned at the right side of the image. A small segment of the image around forward scattering is masked because of the imperfect state selection of the NO packet. The signal intensity within this segment is discarded in all subsequent analysis. We perform full simulations of the experiment to generate the expected scattering image as shown in Figure 2c. In the simulation, we use the theoretically predicted differential cross section and the most relevant experimental parameters such as the spatial, temporal, and velocity spreads of the beams and the ionization volume.[2,17] The simulations therefore include detection bias such as flux to density effects and should reproduce the experimentally obtained image including asymmetries in resolution and signal intensity. A small additional Gaussian blurring of 1 to 2 ms^{-1} is applied to the simulated images to account for the nonperfect velocity mapping conditions and other experimental imperfections.

The experimental and simulated images were analyzed using home written Matlab code to retrieve the angular scattering distributions.[2,4,17] To improve the resolution of the angular scattering distributions, we apply the so-called Finite Slice Analysis method (FinA),[27] which was recently developed by Suits and co-workers, to the raw images. Comparison between the experimental results and the theoretical predictions can now proceed in two ways. In Figure 2b,c, the experimentally obtained angular scattering distribution (red trace) is compared to the DCS as predicted by theory (black dashed trace) and to the angular scattering distribution that follows from the simulated image (blue trace), respectively. All of the angular distributions are normalized for the best overlap. The advantage of the first method is that the experimental results are directly compared to the inherent DCS of the scattering process predicted by theory; the disadvantage however is that both curves are not identical as the experiment blurs part of the structures found in the DCS, and also has an inhomogeneous detection bias with respect to the scattering angles. We therefore prefer to use the second method, as the simulations take these blurring effects into account resulting in two curves that should overlap. We therefore use this method to compare the experimental results with theory throughout, and conclude that both are in agreement if the experimental and simulated images yield the same angular scattering distributions.

From the example presented in Figure 2, it is clear that for NO + *para*-H_2 collisions we are able to resolve the finest structures present in the DCS such as diffraction oscillations. The diffraction peaks have an angular spacing $\Delta\theta$ of about 7.2°, and excellent agreement between experiment and theory is obtained.

3.2. Scattering of NO Radicals with *para*-H_2. In Figure 3, we present our results for inelastic collisions between NO (1/2f) radicals and *para*-H_2 molecules, exciting the NO radicals to the 3/2e, 5/2f, 7/2e, 7/2f, 9/2f, and 11/2e final states. For each final state, the raw experimental image, the simulated image, and the angular distributions that follow from these images after applying FinA reconstruction are shown. For excitation into the lower final rotational states of NO, the angular scattering distribution is dominated by forward scattering and features a clear diffraction pattern. For higher final rotational states, no diffraction oscillations are observed, but a rotational rainbow starts to appear. With increasing values for j' of NO, the angle at which the rainbow is found also increases. In general, excellent agreement between experiment and theory is obtained. The diffraction structures, as well as the intensity and position of the rainbows, are accurately reproduced by the simulations. For the (7/2e) channel, there is a small component near forward scattering that appears more intense in the experiment than in the simulations, but this area is

DOI: 10.1021/acs.jpca.7b06808
J. Phys. Chem. A 2017, 121, 7446−7454

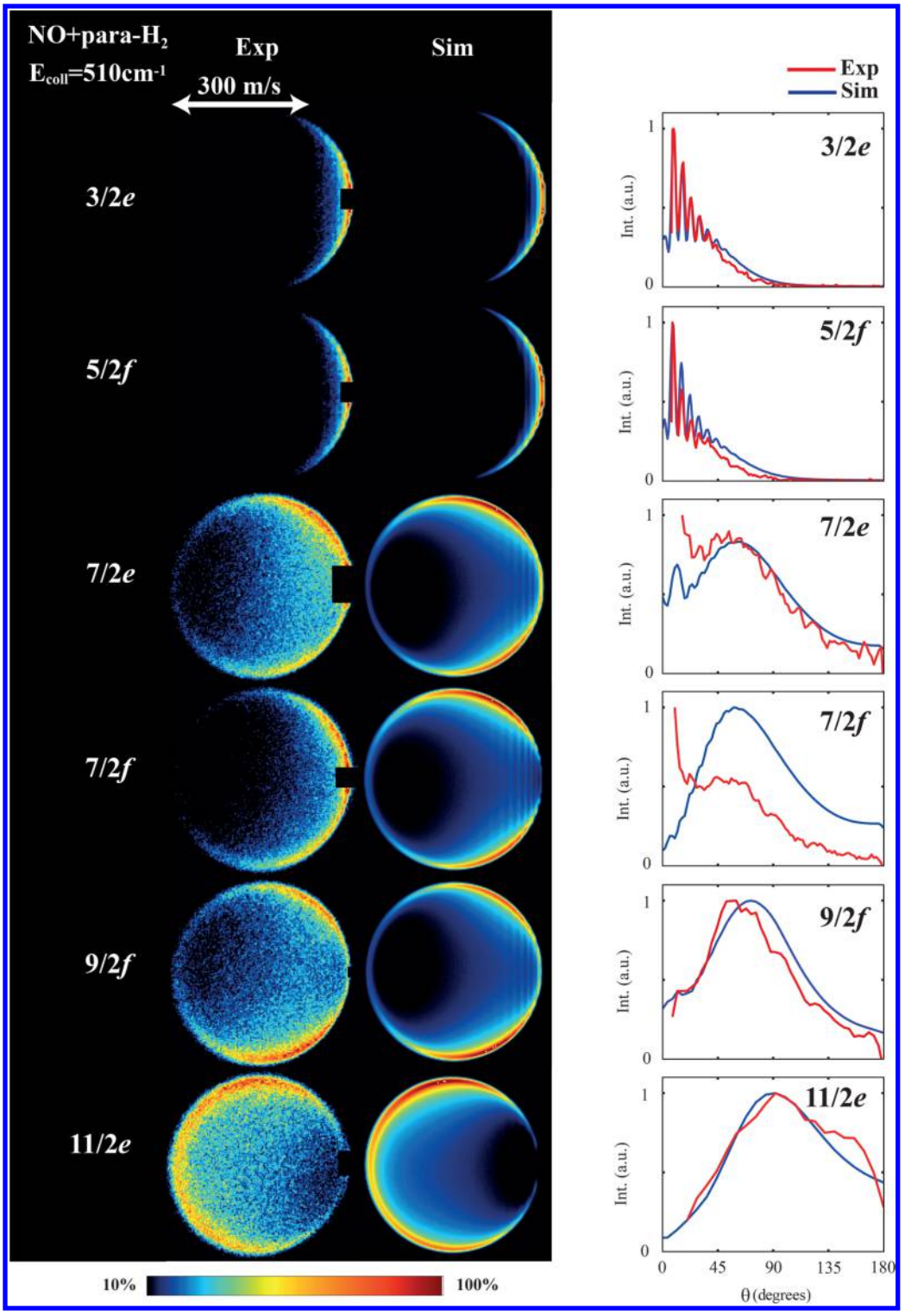

Figure 3. Scattering images for rotational inelastic collisions between NO (1/2f) radicals and *para*-H_2 molecules, exciting the NO radicals to various final states. Left: Experimental (Exp) and simulated (Sim) ion images. Small segments of the images around forward scattering are masked because of the imperfect state selection of the NO packet. Right: Angular scattering distribution as derived from the experimental (red curves) and simulated (blue curves) images.

close to the masked beamspot where our experiment is less sensitive. For the (7/2f) channel, however, the experiment and simulation show a significant discrepancy. The theory predicts a DCS that contains a rainbow at a scattering angle around 60° and very low intensity at near-forward scattered angles. The experiment, by contrast, reveals a distribution that is characterized by a large forward scattered component without a clear rainbow signature. We defer a thorough discussion on this surprising disagreement between experiment and theory for this particular final state to section 3.4.

3.3. Scattering of NO Radicals with *ortho*-D_2. In Figure 4 we report the results of a similar study for NO + *ortho*-D_2 collisions.

DOI: 10.1021/acs.jpca.7b06808
J. Phys. Chem. A 2017, 121, 7446−7454

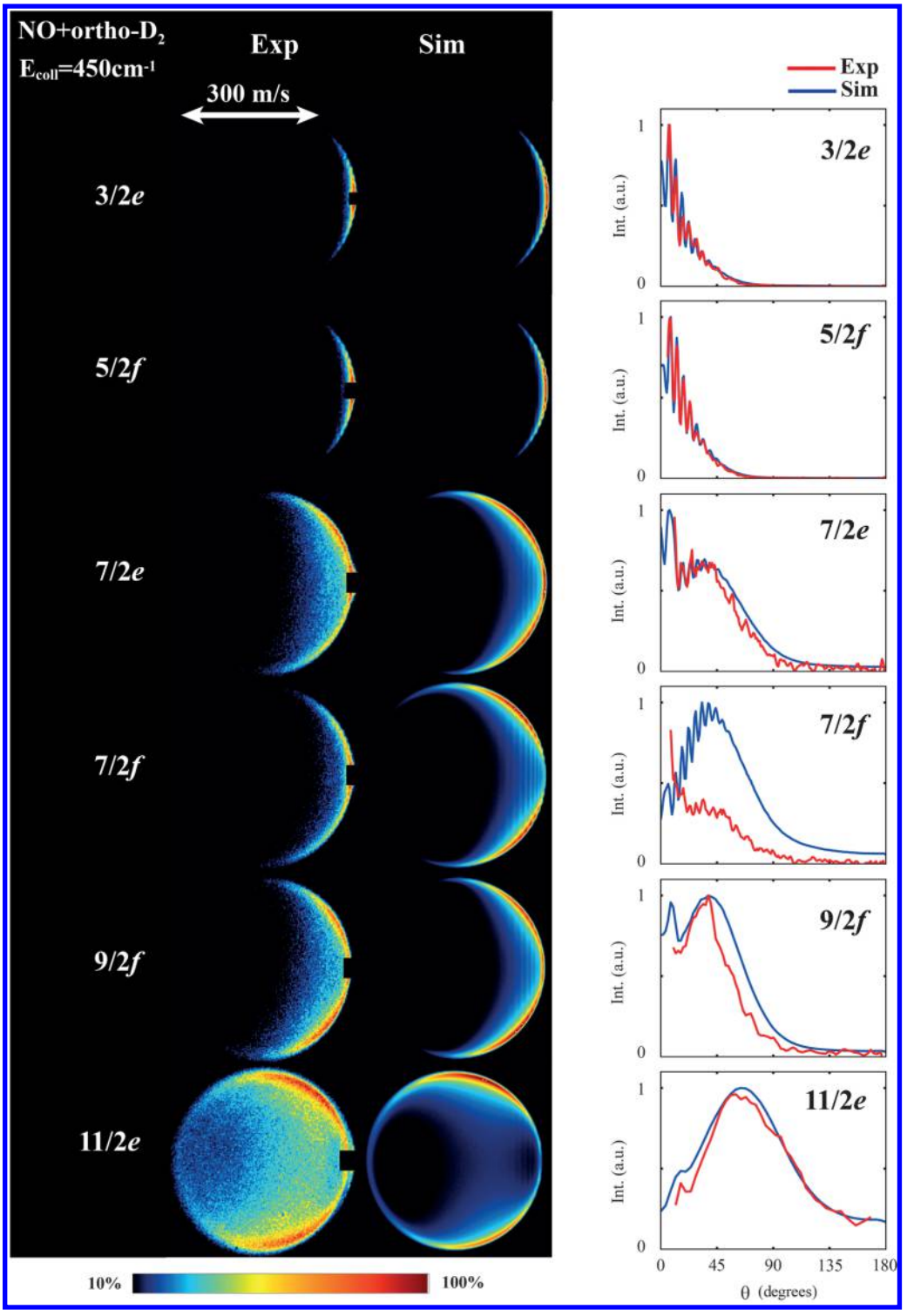

Figure 4. Scattering images for rotational inelastic collisions between NO (1/2f) radicals and *ortho*-D_2 molecules, exciting the NO radicals to various final states. Left: Experimental (Exp) and simulated (Sim) ion images. Small segments of the images around forward scattering are masked because of the imperfect state selection of the NO packet. Right: Angular scattering distribution as derived from the experimental (red curves) and simulated (blue curves) images.

Similar trends in the angular distributions are observed as for NO + *para*-H_2. Excitation to low final states is dominated by forward scattering and diffraction, whereas higher final states feature rainbows at near-side scattered angles. Compared to NO + *para*-H_2 collisions, the diffraction peaks appear closer spaced, and the rainbows have their maximum intensity at smaller angles. Again, excellent agreement between experiment and theory is obtained, except for the (7/2f) channel (see section 3.4 for further discussion).

The main differences that are observed between NO + *para*-H_2 and NO + *ortho*-D_2 can be rationalized using simple semiclassical models for rotational energy transfer. First, we observe a smaller angular spacing between individual diffraction oscillation peaks for NO + D_2 than for NO + *para*-H_2. This difference can be

DOI: 10.1021/acs.jpca.7b06808
J. Phys. Chem. A 2017, 121, 7446−7454

explained by a semiclassical model in which the diffraction structure results from a matter wave that diffracts from a spherical object. As described in detail by Onvlee et al.,[4] the angular spacing $\Delta\theta$ between the diffraction peaks within a hard-sphere scattering model is given by

$$\Delta\theta = \frac{\pi}{kR_0} \quad (1)$$

where k is the wavenumber of the incoming matter wave and R_0 is the radius of the sphere. The collision energy E_{coll} is related to k via $\hbar k = \sqrt{2\mu E_{coll}}$, where μ is the reduced mass of the system (1.88 atomic units for NO−H_2 and 3.53 atomic units for NO−D_2). For both NO + *para*-H_2 and NO + *ortho*-D_2, the radius R can be determined from a spatial contour plot of the interaction potential.[4] An effective radius of the complex then follows the contour with an energy that equals the collision energy of the experiment. This contour is approximated by an ellipse with a minor semiaxis B and two major semiaxes A_N and A_O for the N-end and O-end of the molecule, respectively. Table 1 summarizes

Table 1. Parameters Used for NO+*para*-H_2 and NO+*ortho*-D_2 Collisions To Describe the Angular Spacing of Diffraction Oscillations[a]

	NO + *para*-H_2	NO + *ortho*-D_2
k (a_0)	4.00	5.15
A_O (a_0)	5.67	5.71
A_N (a_0)	6.01	6.05
B (a_0)	4.88	4.91
$\Delta\theta$ (deg) model	7.48	5.8
$\Delta\theta$ (deg) Exp	7.2	5.6

[a]The major (A_N and A_O) and minor (B) semiaxes follow the hard-shell model and are given in units of the Bohr radius (a_0). The angular spacing $\Delta\theta$ between diffraction peaks is calculated by the hard-sphere model ($\Delta\theta$ model) and from the experimentally observed diffraction pattern ($\Delta\theta$ Exp).

the values for k, A_N, A_O, and B that apply to our experimental conditions. Because the NO radical can almost be considered as a homo-nuclear molecule, the values for A_N and A_O are nearly identical. Following the analysis described by Onvlee et al.,[4] we use the largest value to determine R_0. The resulting values for $\Delta\theta$ are in good agreement with the values for the experimentally observed diffraction pattern. From Table 1, it is seen that the different values for $\Delta\theta$ for the two scattering systems mainly originate from the different values for k of the incoming wave.

Second, the scattering angle at which the maximum of a rotational rainbow is found is different for both systems. In a classical picture, the rotational rainbow originates from trajectories with minimal deflection, but where sufficient incoming translational momentum is converted into molecular rotation.[15] The rotational rainbow angle θ_r is expected at[28]

$$\sin\left(\frac{1}{2}\theta_r\right) = \frac{\Delta j}{2k(A_n - B)} \quad (2)$$

where A_n denotes either the semiaxis A_N or A_O introduced before. For the NO radical in the $j = 1/2$f initial state, Δj is approximately equal to $j' + \epsilon'/2$, where Λ-doubling components of e parity have $\epsilon = +1$ and components of f parity have $\epsilon = -1$.

In Table 2, the values for Δj are given for the (9/2, f) and (11/2, e) final states, together with the predicted values for θ_r and the experimentally determined angles at which the rainbows are found. Two rotational rainbows are considered: one from the

Table 2. Parameters Used for NO + *para*-H_2 and NO + *ortho*-D_2 Collisions To Describe the Angle at Which Rotational Rainbows Occur

	NO + *para*-H_2		NO + *ortho*-D_2	
	9/2f	11/2e	9/2f	11/2e
Δj	4	6	4	6
$\theta_{r,O}$ (deg)	78	143	57	92
$\theta_{r,N}$ (deg)	52	82	39	61
$\theta_{r,Exp}$ (deg)	60	92	44	64

N-end and another one from the O-end, described by the rainbow angles $\theta_{r,O}$ and $\theta_{r,N}$. It is seen that the experimentally determined rainbow angle $\theta_{r,Exp}$ is in between the values for $\theta_{r,O}$ and $\theta_{r,N}$. We conclude that, although the hard-shell model is less quantitative, it can qualitatively describe the origins of the rotational rainbow observed here. It is further seen that the rotational rainbow angle decreases with increasing value for k and increases for larger values of Δj, consistent with eq 2.

3.4. Excitation to the 7/2f State. As is clear from the data sets presented in Figures 3 and 4, there is a significant disagreement between experiment and theory for excitation to the 7/2f channel. For this state, we measured a relatively large scattering intensity near forward scattering, whereas this component appears absent in the simulated images. Considering the excellent agreement obtained for all other final states, this disagreement is surprising. In order to investigate the discrepancy, we have performed a number of additional measurements and theoretical calculations. In this section, we summarize these efforts and report their results.

Since the discrepancy only occurs for one specific final state, one may suspect an experimental systematic error related to the detection of population in this final state. We have investigated this experimentally in a number of ways. First, we have studied inelastic collisions between NO radicals with helium atoms under the same experimental conditions, probing various final states. Potential energy surfaces for NO + He[29−31] have already been tested before, and excellent agreement between experiment and theory was found throughout.[6] In Figure 5, the experimental scattering image for the scattering process NO (1/2f) + He → NO (7/2f) + He is shown, together with the simulated results and the angular scattering distributions derived from these images. It is seen that for NO−He there is a good agreement between experiment and theory, although a small shift in rainbow position is observed. Nevertheless, the large forward scattered component that is measured for NO−H_2 and NO−D_2 collisions is not observed for NO−He collisions.

Second, we have studied the scattering process NO (1/2f) + D_2 → NO (7/2f) + D_2 in a different apparatus. Our laboratory operates two independent crossed beam scattering machines that contain identical Stark decelerators, but that use different beam intersection angles, beam sources, lasers, detection units, and data acquisition software. This allows us to revisit experimental results in an unbiased way, unveiling possible systematic errors due to machine-dependent experimental imperfections such as misalignments. Unfortunately, this machine can only operate with normal-D_2, but we will show below that the cross sections for NO + $D_2(j = 0)$, NO + $D_2(j = 1)$, and NO + $D_2(j = 2)$ are very similar. In the lower half of Figure 6, we show the results for a measurement of the process NO (1/2f) + normal-D_2 → NO (7/2f) + normal-D_2, that is measured in a crossed beam scattering apparatus employing a 90° scattering angle, yielding a collision energy of 720 cm^{-1}. This collision energy is higher than

DOI: 10.1021/acs.jpca.7b06808
J. Phys. Chem. A 2017, 121, 7446−7454

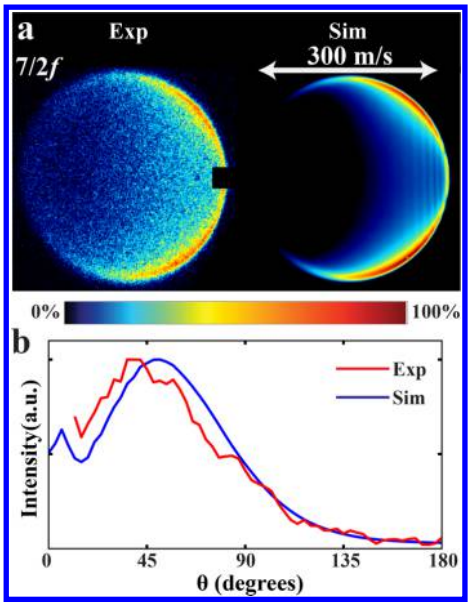

Figure 5. (a) Scattering image for the process NO (1/2f) + He → NO (7/2f) + He, together with a simulated image based on the appropriate DCS predicted by theory. (b) Angular scattering distribution derived from the experimental and simulated images.

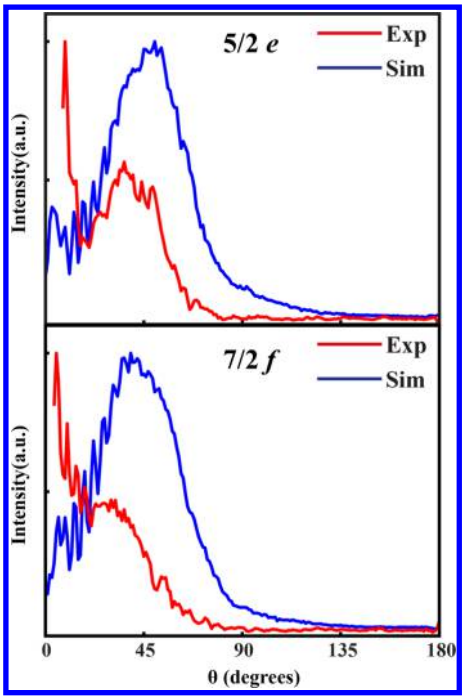

Figure 6. Experimental (Exp) and simulated (Sim) angular scattering distributions for NO + normal-D_2 at a collision energy of 720 cm^{-1}, probing the parity pairs (5/2e) (top) and (7/2f) (bottom).

the energy pertaining to the data presented in Figures 3 and 4, yet the trend of the angular distribution is the same. It features a significant forward scattered component and a relatively weak rainbow feature. The polarization of the laser (226 nm) used in the measurement is vertical. We also changed the polarization of the laser (226 nm) to horizontal; however, hardly any difference was observed. The theoretical calculations for this process, taking the $j = 0$, $j = 1$, and $j = 2$ populations of normal-D_2 into account, again predict an angular distribution featuring a pronounced rainbow and low intensity at forward scattering.

Third, we have studied the scattering process NO (1/2f) + normal-D_2 → NO (5/2e) + normal-D_2. Rotational excitation of NO into the (5/2e) and (7/2f) states are expected to yield almost identical angular distributions, as the DCSs for these two excitations form a so-called parity pair.[15] These measurements are again performed at high collision energy in the apparatus with a 90° crossing angle and directly compared to the measurements probing the (7/2f) final state. The resulting angular distributions for the (5/2e) and (7/2f) states are shown in the upper and lower panels of Figure 6, respectively, together with the theoretical predictions. It is seen that both measurements yield very similar angular distributions, as expected for these parity pairs, but for both states, a significant disagreement with theory is observed.

Since good agreement between experiment and theory is obtained NO + He, one may wonder whether initial population in excited rotational levels of the D_2 molecule can explain the observed scattering behavior, although our measurements using normal-D_2 suggest that initial population in $j = 1$ does not significantly change the scattering behavior. In Figure 7, the

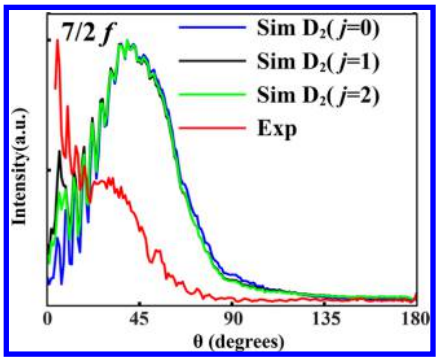

Figure 7. Experimental (Exp) and simulated (Sim) angular scattering distributions for NO + normal-D_2 at a collision energy of 720 cm^{-1}, probing the final state (7/2f). The simulations are performed assuming the hypothetical situation where the D_2 molecules are exclusively in the $j = 0$, $j = 1$, or $j = 2$ rotational states.

angular distributions are shown that are expected from theory for the hypothetical situation in which the D_2 molecules are before the collision exclusively in the $j = 0$ (blue curve), $j = 1$ (black curve), or $j = 2$ state (green curve). The measured angular distribution for the (7/2f) state from Figure 7 is shown again as a comparison. It is seen that population of D_2 in excited rotational levels results in enhanced scattering intensity at forward scattered angles, but not to the extent that it can explain the experimentally observed distributions. It appears highly unlikely that possible minor contaminations of our experiment with D_2 molecules in other initial rotational levels than $j = 0$ can explain the observations.

4. CONCLUSION

We have presented high-resolution measurements of state-to-state differential scattering cross sections for collisions of state-selected NO radicals with *para*-H_2 and *ortho*-D_2 molecules at a collision energy of 510 and 450 cm^{-1}, respectively. Rotational rainbows as well as diffraction oscillations are fully resolved in the angular scattering distributions. In general, the measured distributions are in excellent agreement with the distributions that are predicted by quantum close-coupling scattering calculations, which are based on recently developed NO−H_2 PESs. A significant discrepancy, however, is found for excitation into the (7/2f) state. This discrepancy is found for the scattering partners

DOI: 10.1021/acs.jpca.7b06808
J. Phys. Chem. A 2017, 121, 7446−7454

para-H_2, *ortho*-D_2, and normal D_2. Several additional experiments and calculations have been performed to elucidate the origin of the discrepancy, but no mechanism that can possibly explain the observations could be identified. This is surprising (and perhaps disturbing) in view of the quality of both experiment and theoretical treatments and in view of the excellent agreement that is found for other inelastic channels. There appears either an overlooked systematic error in the experiment or the theoretical calculations are inaccurate. The former appears unlikely considering the agreement that is obtained for NO−He and the similar discrepancy that is found for excitation into the associated parity pair (5/2e). The latter appears unlikely considering the excellent agreement that is obtained for all other final states (and systems that we studied in the past). Further experiments and calculations are warranted to clarify this mystery.

AUTHOR INFORMATION

Corresponding Author

*E-mail: basvdm@science.ru.nl. Phone: +31 243653025.

ORCID

Zhi Gao: 0000-0003-4101-9923

Gerrit C. Groenenboom: 0000-0002-0920-3707

Notes

The authors declare no competing financial interest.

ACKNOWLEDGMENTS

The research leading to these results has received funding from the European Research Council under the European Union's Seventh Framework Programme (FP7/2007−2013)/ERC grant agreement 335646 MOLBIL. This work is part of the research program of The Netherlands Organization for Scientific Research (NWO). The expert technical support by Niek Janssen and André van Roij is gratefully acknowledged.

REFERENCES

(1) Levine, R. D.; Bernstein, R. B. *Molecular Reaction Dynamics and Chemical Reactivity*; Oxford University Press: Oxford, U.K., 1987.

(2) von Zastrow, A.; Onvlee, J.; Vogels, S. N.; Groenenboom, G. C.; van der Avoird, A.; van de Meerakker, S. Y. T. State-Resolved Diffraction Oscillations Imaged for Inelastic Collisions of NO Radicals with He, Ne and Ar. *Nat. Chem.* **2014**, *6*, 216−221.

(3) Brouard, M.; Chadwick, H.; Gordon, S. D. S.; Hornung, B.; Nichols, B.; Aoiz, F. J.; Stolte, S. Stereodynamics in NO(X)+Ar Inelastic Collisions. *J. Chem. Phys.* **2016**, *144*, 224301.

(4) Onvlee, J.; Vogels, S. N.; van der Avoird, A.; Groenenboom, G. C.; van de Meerakker, S. Y. T. Resolving Rainbows with Superimposed Diffraction Oscillations in NO+Rare Gas Scattering: Experiment and Theory. *New J. Phys.* **2015**, *17*, 055019.

(5) Kay, J. J.; Steill, J. D.; Kłos, J.; Paterson, G.; Costen, M. L.; Strecker, K. E.; McKendrick, K. G.; Alexander, M. H.; Chandler, D. W. Collisions of Electronically Excited Molecules: Differential Cross-Sections for Rotationally Inelastic Scattering of NO($A^2\Sigma^+$) with Ar and He. *Mol. Phys.* **2012**, *110*, 1693−1703.

(6) Vogels, S. N.; Onvlee, J.; Chefdeville, S.; van der Avoird, A.; Groenenboom, G. C.; van de Meerakker, S. Y. T. Imaging Resonances in Low-Energy NO-He Inelastic Collisions. *Science* **2015**, *350*, 787−790.

(7) Brouard, M.; Chadwick, H.; Gordon, S. D. S.; Hornung, B.; Nichols, B.; Aoiz, F. J.; Stolte, S. Rotational Orientation Effects in NO(X)+Arx Inelastic Collisions. *J. Phys. Chem. A* **2015**, *119*, 12404−12416.

(8) Brouard, M.; Chadwick, H.; Eyles, C. J.; Hornung, B.; Nichols, B.; Scott, J. M.; Aoiz, F. J.; Kłos, J.; Stolte, S.; Zhang, X. The Fully Quantum State-Resolved Inelastic Scattering of NO(X)+Ne: Experiment and Theory. *Mol. Phys.* **2013**, *111*, 1759−1771.

(9) Brouard, M.; Chadwick, H.; Eyles, C. J.; Hornung, B.; Nichols, B.; Aoiz, F. J.; Jambrina, P. G.; Stolte, S. Rotational Alignment Effects in NO(X)+Ar Inelastic Collisions: An Experimental Study. *J. Chem. Phys.* **2013**, *138*, 104310.

(10) Gijsbertsen, A.; Linnartz, H.; Rus, G.; Wiskerke, A. E.; Stolte, S.; Chandler, D. W.; Kłos, J. Differential Cross Sections for Collisions of Hexapole State-Selected NO with He. *J. Chem. Phys.* **2005**, *123*, 224305.

(11) van Leuken, J. J.; van Amerom, F. H. W.; Bulthuis, J.; Snijders, J. G.; Stolte, S. Parity-Resolved Rotationally Inelastic Collisions of Hexapole State-Selected NO ($^2\Pi_{1/2}$, $J = 1/2^-$) with Ar. *J. Phys. Chem.* **1995**, *99*, 15573−15579.

(12) Nichols, B.; Chadwick, H.; Gordon, S. D. S.; Eyles, C. J.; Hornung, B.; Brouard, M.; Alexander, M. H.; Aoiz, F. J.; Gijsbertsen, A.; Stolte, S. Steric Effects and Quantum Interference in the Inelastic Scattering of NO(X)+Ar. *Chem. Sci.* **2015**, *6*, 2202−2210.

(13) Kirste, M.; Wang, X.; Schewe, H. C.; Meijer, G.; Liu, K.; van der Avoird, A.; Janssen, L. M. C.; Gubbels, K. B.; Groenenboom, G. C.; van de Meerakker, S. Y. T. Quantum-State Resolved Bimolecular Collisions of Velocity-Controlled OH with NO Radicals. *Science* **2012**, *338*, 1060−1063.

(14) Westley, M. S.; Lorenz, K. T.; Chandler, D. W.; Houston, P. L. Differential Cross Sections for Rotationally Inelastic Scattering of NO from He and D_2. *J. Chem. Phys.* **2001**, *114*, 2669−2680.

(15) Gijsbertsen, A.; Linnartz, H.; Stolte, S. Parity-Dependent Rotational Rainbows in D_2−NO and He−NO Differential Collision Cross Sections. *J. Chem. Phys.* **2006**, *125*, 133112.

(16) Luxford, T. F. M.; Sharples, T. R.; Townsend, D.; McKendrick, K. G.; Costen, M. L. Comparative Stereodynamics in Molecule-Atom and Molecule-Molecule Rotational Energy Transfer: NO($A^2\Sigma^+$)+He and D_2. *J. Chem. Phys.* **2016**, *145*, 084312.

(17) de Jongh, T.; Karman, T.; Vogels, S. N.; Besemer, M.; Onvlee, J.; Suits, A. G.; Thompson, J. O. F.; Groenenboom, G. C.; van der Avoird, A.; van de Meerakker, S. Y. T. Imaging Diffraction Oscillations for Inelastic Collisions of NO Radicals with He and D_2. *J. Chem. Phys.* **2017**, *147*, 013918.

(18) Pajón-Suárez, P.; Valentín-Rodríguez, M.; Hernández-Lamoneda, R. The Interaction Potential of NO−H_2 in Ground and A Rydberg State. *Chem. Phys. Lett.* **2016**, *658*, 176−181.

(19) Kłos, J.; Ma, Q.; Alexander, M. H.; Dagdigian, P. J. The Interaction of NO($X^2\Pi$) with H_2: *Ab Initio* Potential Energy Surfaces and Bound States. *J. Chem. Phys.* **2017**, *146*, 114301.

(20) Onvlee, J.; Vogels, S. N.; von Zastrow, A.; Parker, D. H.; van de Meerakker, S. Y. T. Molecular Collisions Coming into Focus. *Phys. Chem. Chem. Phys.* **2014**, *16*, 15768−15779.

(21) van de Meerakker, S. Y. T.; Bethlem, H. L.; Vanhaecke, N.; Meijer, G. Manipulation and Control of Molecular Beams. *Chem. Rev.* **2012**, *112*, 4828−4878.

(22) van de Meerakker, S. Y. T.; Vanhaecke, N.; Bethlem, H. L.; Meijer, G. Higher-Order Resonances in a Stark Decelerator. *Phys. Rev. A: At., Mol., Opt. Phys.* **2005**, *71*, 053409.

(23) Wang, X.; Kirste, M.; Meijer, G.; van de Meerakker, S. Y. T. Stark Deceleration of NO Radicals. *Z. Phys. Chem.* **2013**, 130617035227002.

(24) Yan, B.; Claus, P. F. H.; van Oorschot, B. G. M.; Gerritsen, L.; Eppink, A. T. J. B.; van de Meerakker, S. Y. T.; Parker, D. H. A New High Intensity and Short-Pulse Molecular Beam Valve. *Rev. Sci. Instrum.* **2013**, *84*, 023102.

(25) Townsend, D.; Minitti, M. P.; Suits, A. G. Direct Current Slice Imaging. *Rev. Sci. Instrum.* **2003**, *74*, 2530−2539.

(26) Groenenboom, G. C.; Fishchuk, A. V.; van der Avoird, A. Bound States of the OH($^2\Pi$)-HCl Complex on *Ab Initio* Diabatic Potentials. *J. Chem. Phys.* **2009**, *131*, 124307.

(27) Thompson, J. O. F.; Amarasinghe, C.; Foley, C. D.; Suits, A. G. Finite Slice Analysis (FINA)−A General Reconstruction Method for Velocity Mapped and Time-Sliced Ion Imaging. *J. Chem. Phys.* **2017**, *147*, 013913.

(28) Bosanac, S. Two-Dimensional Model of Rotationally Inelastic Collisions. *Phys. Rev. A: At., Mol., Opt. Phys.* **1980**, *22*, 2617−2622.

(29) Yang, M.; Alexander, M. H. *Ab Initio* Potential Energy Surfaces and Quantum Scattering Studies of NO($X^2\Pi$) with He: Λ-Doublet

DOI: 10.1021/acs.jpca.7b06808
J. Phys. Chem. A 2017, 121, 7446−7454

Resolved Rotational and Electronic Fine-Structure Transitions. *J. Chem. Phys.* **1995**, *103*, 6973−6983.
(30) Kłos, J.; Chałasinski, G.; Berry, M. T.; Bukowski, R.; Cybulski, S. M. *Ab Initio* Potential-Energy Surface for the He(^1S)+ NO($X^2\Pi$) Interaction and Bound Rovibrational States. *J. Chem. Phys.* **2000**, *112*, 2195−2203.
(31) Onvlee, J.; van der Avoird, A.; Groenenboom, G.; van de Meerakker, S. Y. T. Probing Scattering Resonances in (Ultra)Cold Inelastic NO-He Collisions. *J. Phys. Chem. A* **2016**, *120*, 4770−4777.

DOI: 10.1021/acs.jpca.7b06808
J. Phys. Chem. A 2017, 121, 7446−7454